Excitation functions of ^{45}Sc-induced reactions: towards future superheavy element synthesis

T. A. Werke, D. A. Mayorov, M. C. Alfonso, M. E. Bennett, and C. M. Folden III

The study of fusion-evaporation reactions at near-Coulomb barrier energies is critical to understanding the production of heavy and superheavy elements (SHEs). Using a ^{48}Ca (Z = 20) beam on actinide targets, elements with Z = 113 - 118 have been synthesized by the Dubna-Livermore Collaboration [1-4]. A lack of available target material means that beams with Z > 20 such as ^{45}Sc must be developed to produce the next SHEs. Very little experimental data exists on fusion evaporation cross sections using a ^{45}Sc beam. By experimentally measuring excitation functions of ^{45}Sc-induced reactions on lanthanide targets, we can study the effects of changing the projectile from ^{48}Ca to the much less neutron-rich ^{45}Sc. These studies will also provide insight towards the likelihood of producing superheavy elements with ^{45}Sc projectiles.

The heavy elements group at Texas A&M University has studied intermediate mass fusion-evaporation reactions using a metal beam with Z ≥ 20 bombarding lanthanide targets to produce actinides near the N = 126 shell. Heavy ion fusion-evaporation reactions have been studied using ^{45}Sc projectiles accelerated by the K500 cyclotron at the Cyclotron Institute. The reaction systems were selected with several desirable properties in mind, such as large alpha-decay branches and short half-lives [5,6]; see Table I for details. Beam energies were varied using a series of ^{nat}Al degraders with thicknesses of 0 (no degrader), 1.2, 2.25, 3.45, 4.5, 5.1, and 6.29 μm. The beam dose was monitored by Rutherford scattering on two circular silicon detectors at ±30° to the beam axis in the target chamber. The ^{45}Sc primary beam bombarded a self-supporting target of 498-μg/cm^2 ^{159}Tb, and a 403-μg/cm^2 ^{162}Dy target that is supported by 75-μg/cm^2 ^{nat}C. Unreacted primary beam and unwanted reaction products were separated using the Momentum Achromat Recoil Spectrometer (MARS) [7]. MARS filters products using a two stage scheme consisting of an achromatic magnetic rigidity selection section followed by a Wien Filter. The separation factor of primary beam and unwanted reaction products is approximately on the level of 10^{15} [8]. Evaporation residues were tuned through MARS and implanted in a single focal plane silicon strip detector. A microchannel plate detector serves as a veto detector to discriminate implants from the subsequent alpha decays. Preliminary results are reported here.

Table I. Selected properties for the reactions of ^{45}Sc +^{159}Tb, ^{162}Dy and ^{48}Ca +^{159}Tb. N_{CN} is the number of neutrons in the compound nucleus. Z_pZ_t is the charge product of the projectile and target nuclei. The half-life and alpha branching ratio (b_α) are given for the 4n evaporation residue (EvR). σ_{calc} is the predicted maximum cross section for the 4n EvR calculated by the method of Zagrebaev *et al.* in [9,10]. Half-lives are taken from [5]. Alpha branching ratios are taken from [6].

Projectile	Target	CN	N_{CN}	Z_pZ_t	$t_{1/2}$ (s)	b_α (%)	σ_{calc} (mb)
^{45}Sc	^{159}Tb	^{204}Rn	118	1365	$1.03^{+020}_{-0.11}$	86^{+14}_{-4}	0.46
^{45}Sc	^{162}Dy	^{207}Fr	120	1386	0.55 ±0.01	95 ± 5*	0.14
^{48}Ca	^{159}Tb	^{207}At	122	1300	444 ± 12	31 ± 3	14

* No uncertainty given. Value estimated from [6].

Experimental data have been collected for the reaction systems of ^{45}Sc + ^{159}Tb, ^{162}Dy and are shown in Figs. 1 and 2, where E_{cot} is the center-of-target beam energy in the laboratory frame**.** The figures also show excitation functions for other similar reactions on the same targets. The data show that reactions using ^{45}Sc projectiles have cross sections that are two orders of magnitude less than the theoretical calculations using the method of Zagrebaev [9,10], and that are three orders of magnitude less than ^{48}Ca-induced reactions on the same target.

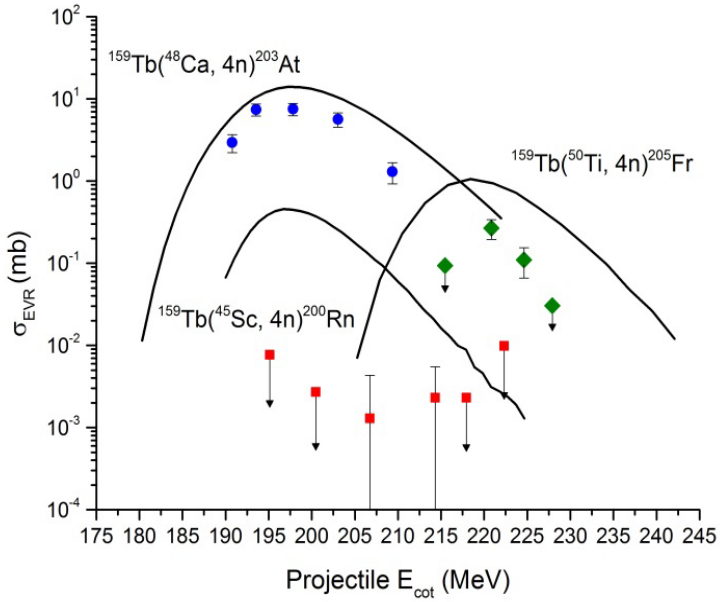

FIG. 1. Excitation functions for projectiles of ^{48}Ca, ^{45}Sc, and ^{50}Ti on a ^{159}Tb target. Solid lines are theoretical predictions from Zagrebaev *et al.*[9,10].

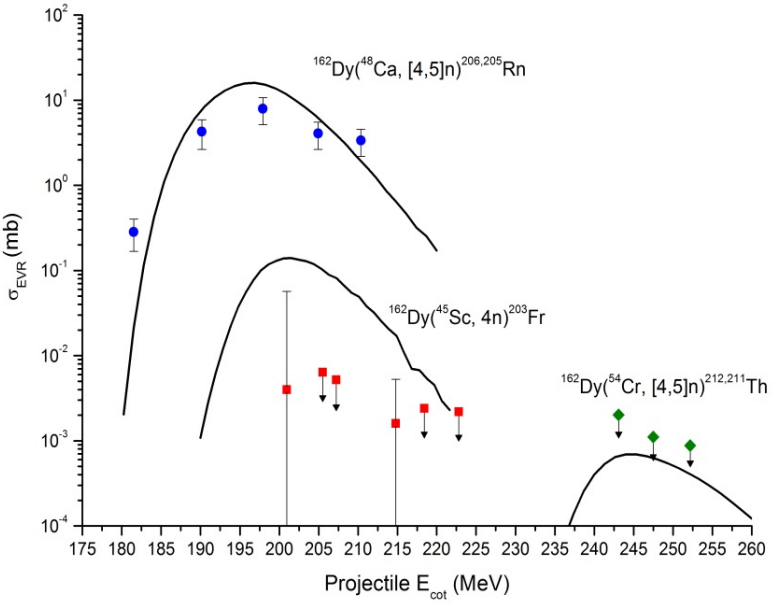

FIG. 2. Excitation functions for projectiles of ^{48}Ca, ^{45}Sc, and ^{54}Cr on a ^{162}Dy target. Solid lines are theoretical predictions from Zagrebaev *et al.* [9,10].

The theoretical description of the fusion-evaporation process is almost universally presented as a progression of three steps, shown in Fig. 3**.** The projectile-target system overcomes an interaction barrier and comes into contact, evolves into a single excited nucleus, and finally decays by several nucleon evaporations (the 4n channel is depicted in Fig. 3) and gamma emission into the ground state. The

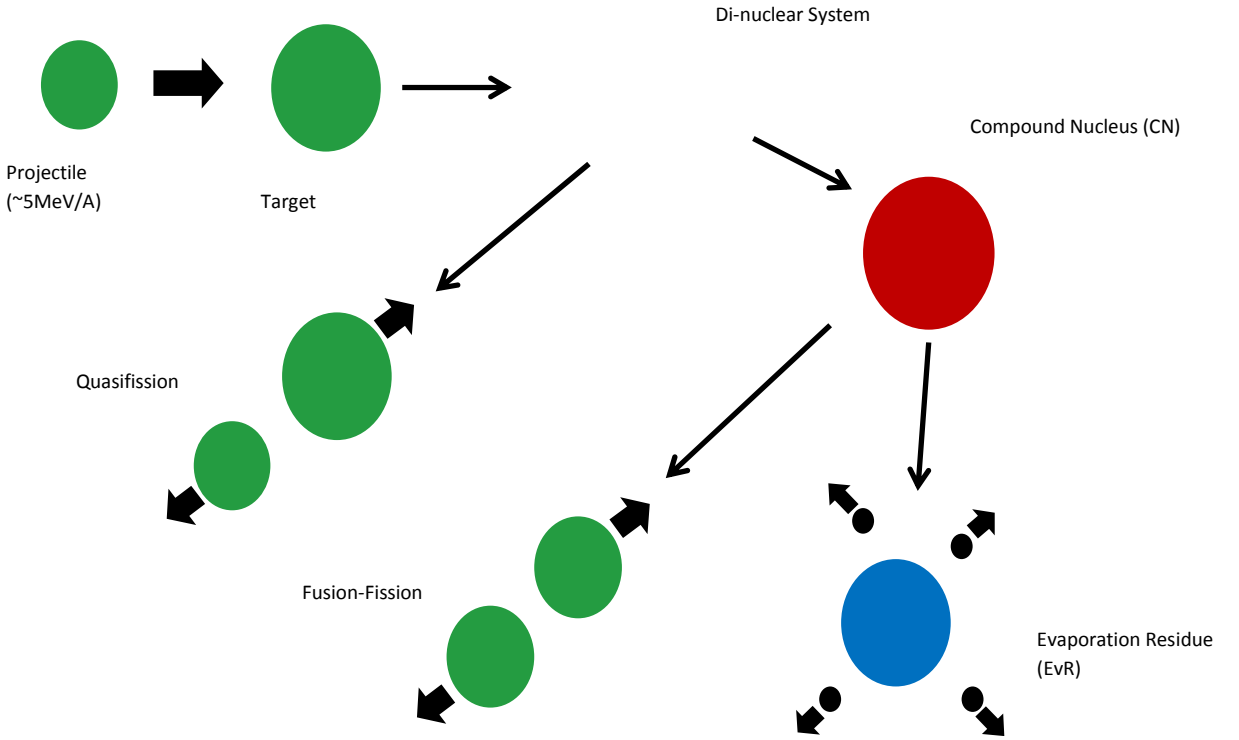

FIG. 3. Depiction of the fusion-evaporation process. The projectile and target capture and fuse to form the compound nucleus (CN). The CN de-excites via nucleon emissions to give the evaporation residue (EvR).

fusion-evaporation cross section is commonly represented as the product of three terms [11]:

$$\sigma_{EvR} = \sigma_{capt}(E) P_{CN}(E^*, l) P_{xn}(E^*, l) \qquad (1)$$

where E is the center of mass projectile energy, E* is the excitation energy of the compound nucleus, and l is the angular momentum of the compound system. $\sigma_{capt}(E)$ is the capture cross section for the projectile to overcome the interaction barrier and form a di-nuclear system. $P_{CN}(E^*, l)$ is the probability of forming the compound nucleus, and $P_{xn}(E^*, l)$ is the probability of the compound nucleus evaporating x neutrons and reaching the ground state of the evaporation residue. The large reduction in 4n EvR cross section for the ^{45}Sc-induced reactions must arise from one of the three terms in equation (1). $\sigma_{capt}(E)$ is relatively well understood and can be calculated within a factor of two [1,2]. Values of $\sigma_{capt}(E)$ for the reactions in Figs. 1 and 2 are calculated using the method of Zagrebaev *et al.* [9] and are shown in Table II. These data indicate that $\sigma_{capt}(E)$ changes by about a factor of 1.5, which is not enough to account for the three orders of magnitude difference in the EvR cross sections. $P_{CN}(E^*, l)$ depends on the charge

product of the target and projectile, Z_pZ_t. Table I shows that the values of Z_pZ_t change by less than 5% from ^{48}Ca beam to ^{45}Sc beam, and previous data suggests that $P_{CN}(E^*, l)$ should have a value between 0.25 to 1 for the reaction systems [13]. This is also insufficient to account for the three orders of magnitude difference in the EvR cross sections between the ^{48}Ca-induced reactions and the ^{45}Sc-induced reactions.

Table II. Calculated values of the capture cross section for the reactions in Figs. 2 and 3 using the method of Zagrebaev *et al.* [9].

Reaction	$\sigma_{capt}(E)$ (mb)
^{48}Ca+^{159}Tb	378
^{45}Sc+^{159}Tb	214
^{50}Ti+^{159}Tb	431
^{48}Ca+^{162}Dy	420
^{45}Sc+^{162}Dy	341
^{54}Cr+^{162}Dy	449

The final quantity in Eq. (1), $P_{xn}(E^*, l)$, depends on the decay widths for neutron emission, Γ_n, and fission, Γ_f, as shown in Eq. (2).

$$P_{xn}(E^*, l) = P(x, E^*) \prod_{i=1}^{x} \left(\frac{\Gamma_n}{\Gamma_n + \Gamma_f}\right)_{i,E^*,l} \quad (2)$$

$P(x, E^*)$ denotes the probability for emitting exactly x neutrons. Using transition state theory, the dependence of the quantity Γ_n/Γ_f on the neutron binding energy, B_n, and the fission barrier, B_f [14,15] can be shown:

$$\frac{\Gamma_n}{\Gamma_f} \propto \exp[2a_n^{\frac{1}{2}}(E^* - B_n)^{\frac{1}{2}} - 2a_f^{\frac{1}{2}}(E^* - B_f)^{\frac{1}{2}}] \quad (3)$$

where a_n and a_f are the level density parameters for neutron emission and fission, respectively. A small neutron binding energy and a large fission barrier increases the probability of the excited CN emitting neutrons to give the desired EvR. Due the exponential dependence in Eq. (3), small changes in $B_n - B_f$ result in a large change to Γ_n/Γ_f. The factor Γ_n/Γ_f is then taken to the power of x, further amplifying the effects of $B_n - B_f$ on $P_{xn}(E^*, l)$. The data show that the ^{48}Ca-induced reactions have values of $B_n - B_f$ that are 7 MeV more negative than the corresponding ^{45}Sc-induced reactions as shown in Fig. 4. This result is due to the relative neutron deficiency of ^{45}Sc projectiles compared to the neutron rich ^{48}Ca projectile. In the CN, neutron deficiency means a larger neutron binding energy and a smaller fission barrier; both of these effects work against the likelihood of neutron emission. This result likely explains the majority of the three orders of magnitude difference in the 4n EvR cross sections between the ^{48}Ca-induced reactions and the ^{45}Sc-induced reactions.

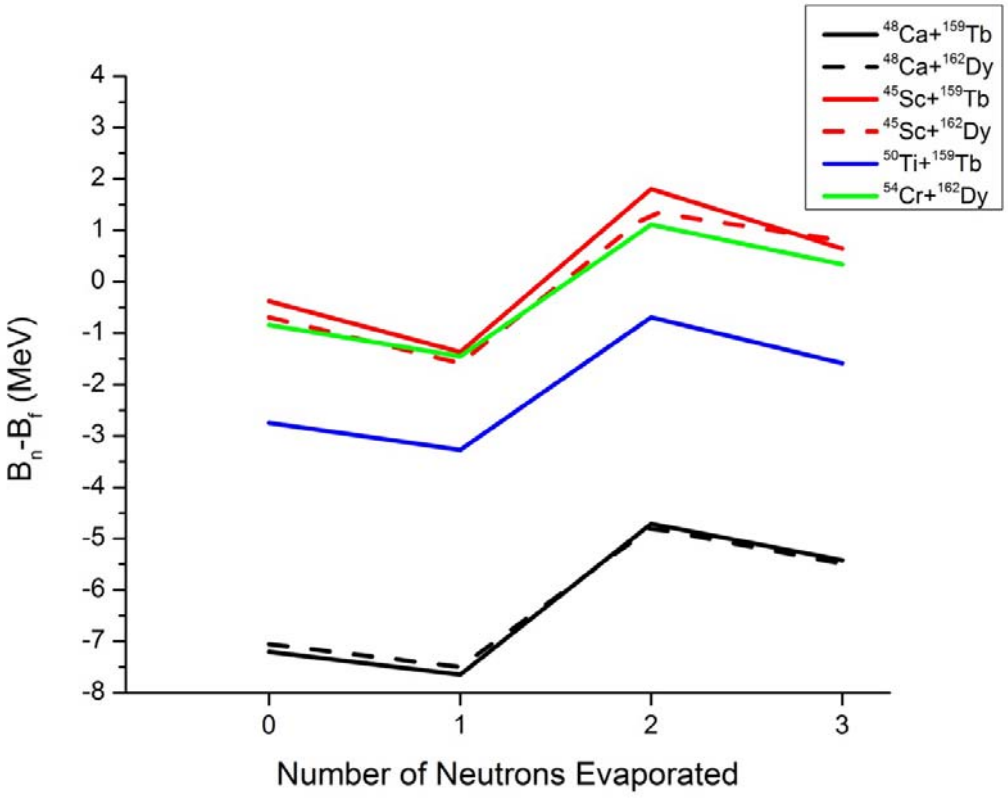

FIG. 4. Values of B_n-B_f for the reaction systems in Figs 2 and 3.

Complete fusion evaporation cross sections have been measured for reactions of ^{45}Sc + ^{159}Tb, ^{162}Dy at Texas A&M University. The cross sections are three orders of magnitude lower than cross sections for ^{48}Ca projectiles on the same target. The relative neutron deficiency of ^{45}Sc compared to ^{48}Ca results in a large reduction in the survival probability for the ^{45}Sc-induced reactions and likely accounts for the majority of the difference in EvR cross sections. This suggests that ^{45}Sc-induced reactions will likely have very small cross sections for the production of new SHEs. ^{50}Ti-induced reactions will create more neutron-rich compound nuclei and likely result in larger EvR cross sections. Future experiments will revisit the ^{45}Sc beam reactions, as well as use other metal beams with $Z \geq 20$ on lanthanide targets to help to better quantify these effects.

[1] Y. Oganessian, J. Phys. G. **34**, R165 (2007).
[2] Y.T. Oganessian *et al.*, Phys. Rev. C **74**, 044602 (2006).
[3] Y.T. Oganessian *et al.*, Phys. Rev. Lett. **104**, 142502 (2010).
[4] Y.T. Oganessian *et al.*, Phys. Rev. C **72**, 034611 (2005).
[5] National Nuclear Data Center, *Chart of the Nuclides*; available at http://www.nndc.bnl.gov/.

[6] R.B. Firestone and L.P. Ekstrom, *WWW Table of Radioactive Isotopes - Nuclide Search*; available at http://ie.lbl.gov/toi/nucSearch.asp.
[7] R.E. Tribble, R.H. Burch, and C.A. Gagliardi, Nucl. Instrum. Methods Phys. Res. **A285**, 441 (1989).
[8] C.M. Folden III *et. al.*, Nucl. Instrum. Methods Phys. Res. **A678**, 1 (2012).
[9] V. Zagrebaev *et. al.*, *Empirical model code of the NRV*; available at http://nrv.jinr.ru/nrv/.
[10] V. Zagrebaev *et. al.*, *Monte Carlo code of the NRV*; available at http://nrv.jinr.ru/nrv/.
[11] V. Zagrebaev and W. Greiner, Phys. Rev. C **78**, 034610 (2008).
[12] W. Loveland, arxiv:1207.2095v1 (2012).
[13] C.M. Folden III *et. al.* , J. Phys.: Conf. Ser. **420** 012007 (2012).
[14] A.J. Sierk, Phys. Rev. C **33** (1986).
[15] W.D. Myers and W. J. Swiatecki, *Table of Nuclear Masses according to the 1994 Thomas-Fermi Model*; available at http://ie.lbl.gov/txt/ms.txt.